ARMY RESEARCH LABORATORY

# Adaptive Deblurring of Noisy Images

**by S. Susan Young, Ronald G. Driggers,
Brian P. Teaney, and Eddie L. Jacobs**

**ARL-TR-4276** **October 2007**

## NOTICES

### Disclaimers

The findings in this report are not to be construed as an official Department of the Army position unless so designated by other authorized documents.

Citation of manufacturer's or trade names does not constitute an official endorsement or approval of the use thereof.

Destroy this report when it is no longer needed. Do not return it to the originator.

# Army Research Laboratory
Adelphi, MD 20783-1197

**ARL-TR-4276** **October 2007**


# Adaptive Deblurring of Noisy Images


**S. Susan Young**
**U.S. Army Research Laboratory**
**Sensors and Electron Devices Directorate**

**Ronald G. Driggers, Brian P. Teaney**
**Night Vision and Electronic Sensors Directorate**

**Eddie L. Jacobs**
**The University of Memphis**

# REPORT DOCUMENTATION PAGE

*Form Approved*
*OMB No. 0704-0188*



| 1. REPORT DATE *(DD-MM-YYYY)* | 2. REPORT TYPE | 3. DATES COVERED (From - To) |
|---|---|---|
| October 2007 | Final | June 2006 to September 2007 |

**4. TITLE AND SUBTITLE**
Adaptive Deblurring of Noisy Images

**5a. CONTRACT NUMBER**

**5b. GRANT NUMBER**

**5c. PROGRAM ELEMENT NUMBER**

**6. AUTHOR(S)**
S. Susan Young, Ronald G. Driggers, Brian P. Teaney, and Eddie L. Jacobs

**5d. PROJECT NUMBER**

**5e. TASK NUMBER**

**5f. WORK UNIT NUMBER**

**7. PERFORMING ORGANIZATION NAME(S) AND ADDRESS(ES)**
U.S. Army Research Laboratory
ATTN: AMSRD-ARL-SE-SE
2800 Powder Mill Road
Adelphi, MD 20783-1197

**8. PERFORMING ORGANIZATION REPORT NUMBER**
ARL-TR-4276

**9. SPONSORING/MONITORING AGENCY NAME(S) AND ADDRESS(ES)**
U.S. Army Research Laboratory
2800 Powder Mill Road
Adelphi, MD 20783-1197

Night Vision and Electronic Sensors Directorate
Fort Belvoir, VA 22060

**10. SPONSOR/MONITOR'S ACRONYM(S)**

**11. SPONSOR/MONITOR'S REPORT NUMBER(S)**
ARL-TR-4276

**12. DISTRIBUTION/AVAILABILITY STATEMENT**
Approved for public release; distribution unlimited.

**13. SUPPLEMENTARY NOTES**

**14. ABSTRACT**

This report proposes a practical sensor deblur filtering method for images that are contaminated with noise. A sensor blurring function is usually modeled via a Gaussian-like function having a bell shape. The straightforward inverse function results in magnification of noise at the high frequencies. In order to address this issue, we apply a special spectral window to the inverse blurring function. This special window is called the *power* window, which is a Fourier-based smoothing window that preserves most of the spatial frequency components in the passband and attenuates quickly at the transition-band. The power window is differentiable at the transition point which gives a desired smooth property and limits the ripple effect. Utilizing properties of the power window, we design the deblurring filter adaptively by estimating energy of the signal and noise of the image to determine the passband and transition-band of the filter. The deblurring filter design criteria are: a) filter magnitude is less than one at the frequencies where the noise is stronger than the desired signal (transition-band); and b) filter magnitude is greater than one at the other frequencies (passband). Therefore, the adaptively designed deblurring filter is able to deblur the image by a desired amount based on the estimated or known blurring function while suppressing the noise in the output image. The deblurring filter performance is demonstrated by a human perception experiment which 10 observers are to identify 12 military targets with 12 aspect angles. The results of comparing target identification probabilities with blurred, deblurred, adding 2 level of noise to blurred, and deblurred noisy images are reported.

**15. SUBJECT TERMS**
Deblurring filter, adaptive design, noise suppression, human perception study

| 16. SECURITY CLASSIFICATION OF: | | | 17. LIMITATION OF ABSTRACT | 18. NUMBER OF PAGES | 19a. NAME OF RESPONSIBLE PERSON |
|---|---|---|---|---|---|
| a. REPORT | b. ABSTRACT | c. THIS PAGE | | | S. Susan Young |
| U | U | U | SAR | 30 | 19b. TELEPHONE NUMBER (*Include area code*) (301) 394-0230 |

## Contents

## List of Figures and Table

# 1. Introduction

The image acquisition model, shown in figure 1a, demonstrates the measurement model for the measured signal or image $r(x, y)$ via the output of a Linear Shift Invariant (LSI) system whose impulse response is the sensor's point spread function (PSF) $g(x, y)$; the latter is also known as the sensor blurring function. The signal $n(x, y)$ is the additive noise. The observed signal or image $r(x, y)$ is the sum of the noise and the convolution of the sensor blurring function $g(x, y)$ with the "true" signal or image $f(x, y)$:

$$r(x, y) = f(x, y) \otimes g(x, y) + n(x, y). \tag{1}$$

The convolution relation in the spatial frequency domain $(k_x, k_y)$ is written as follows:

$$R(k_x, k_y) = F(k_x, k_y) \cdot G(k_x, k_y) + N(k_x, k_y) \tag{2}$$

where $R(k_x, k_y)$, $F(k_x, k_y)$, $G(k_x, k_y)$, and $N(k_x, k_y)$ are the Fourier transforms of $r(x, y)$, $f(x, y)$, $g(x, y)$, and $n(x, y)$, respectively. The blurring function $G(k_x, k_y)$, in most practical imaging systems, is a radially symmetric function. In that case, if the radial spatial frequency domain is defined to be

$$\rho = \sqrt{k_x^2 + k_y^2}, \tag{3}$$

the blurring function can be identified as $G(\rho)$. The blurring function $G(\rho)$ is typically a low-pass filter (e.g., Gaussian). The noise $n(x, y)$ is a white process, i.e., the spectrum $|N(\rho)|^2$ has a wide-bandwidth (flat) support band as shown in figure 1b.

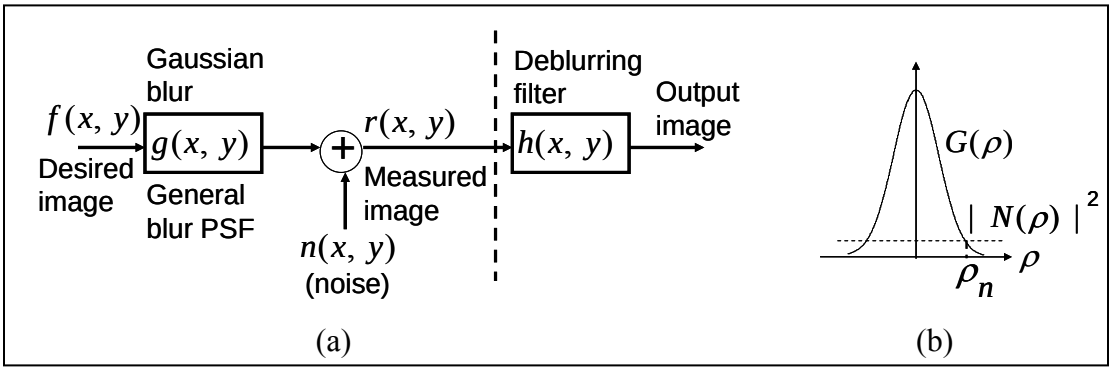


Figure 1. (a) Image acquisition model, and (b) noise spectrum support band.

The deblurring process is to recover $f(x, y)$ from the measured signal $r(x, y)$ by applying the deblurring filter $h(x, y)$ (figure 1a). This process is also called deconvolution or restoration (*1–3*). The straightforward deblurring filter is the inverse of the blurring function.

When we apply this kind of deblurring filter, we have,

$$\frac{R(\rho)}{G(\rho)} = F(\rho) + \frac{N(\rho)}{G(\rho)}. \tag{4}$$

The second term usually blows up (becomes unstable) at the high frequencies where the signal level $|F(\rho)|$ is below the noise level $|N(\rho)|$.

Several recently reviewed journal articles (*4–7*) have summarized the research that attempts to solve this problem. Demoment quotes, "Everything was summed up in a single word: regularization" (*4*). Deblurring is an ill-posed inverse problem due to the above-mentioned instability. For ill-posed (or ill-conditioned) problems, obtaining the true solution from imperfect data is impossible. Regularization is a general principle to obtain an acceptable solution by incorporating some extra or *a prior* information of the imaging system.

In summary, regularization is a method that *a prior* knowledge of the imaging systems (e.g., PSF of the system) or assumption of the true image [$f(x, y)$] is utilized to form a risk function. The risk function is then solved by different implementations of the non-linear optimization problems, such as the gradient-based method, expectation-maximization (EM) technique, prediction error-based technique, and least square methods. Recent research (*8, 9*) differs in the assumptions about the true image and PSF, and how these assumptions are imposed in forming different risk functions. An example is that searching the solution of $f(x, y)$ value which maximizes the *a posterior* (MAP) distribution

$$f(x, y) = \arg\max\, p[f(x, y)|r(x, y)]. \tag{5}$$

Usually, the risk function depends on the actual object which is unknown. An appropriate solution has to be chosen through proper initialization of the algorithm. Because of the nature of non-linear optimization problems, there is a chance that the methods may converge to local minima. In addition, the convergence speed may be slow.

Additionally, recent research has been using the various implementations of the Wiener filter approach. The Wiener filter is defined as

$$H_{wiener}(\rho) = \frac{G(\rho)^*}{|G(\rho)|^2 + S_n(\rho) / S_f(\rho)} \tag{6}$$

where $S_f(\rho)$ and $S_n(\rho)$ are the signal and noise power spectral densities, respectively. Theoretically, the Wiener filter is the optimal linear filter (in Root Mean Square Error (RMSE) sense). The problem with the Wiener filter is that its parameters (degradation function and signal to noise ratio (SNR)) are not always known and in such case, it suffers from limitations such as those to be discussed next.

When the noise power is weak ($S_n(\rho)/S_f(\rho) << 1$), the Wiener filter becomes $1/G(\rho)$, that is, pseudoinverse of $G(\rho)$, which has the instability problems previously mentioned. Theoretically, if $G(\rho)$ and the SNR are known precisely, then the instability is negligible (in RMSE sense) since the noise is negligible. However, in practice the SNR and $G(\rho)$ are not known precisely and the estimated inverse filter $1/G(\rho)$ may be instable because of small errors in the estimated filter parameters. On the other hand, when the noise is strong ($S_n(\rho)/S_f(\rho) >> 1$), the Wiener filter becomes $G(\rho)^*/[S_n(\rho)/S_f(\rho)]$, that is proportional to the SNR, which filters noise, but not effective for deblurring.

The parametric Wiener filter is implemented using the parameter $\gamma$ in the following definition:

$$H_{wiener}(\rho) = \frac{G(\rho)^*}{|G(\rho)|^2 + \gamma\, S_n(\rho) / S_f(\rho)}. \tag{7}$$

The effect of $\gamma$ on the filter tends to emphasize ($\gamma > 1$) or de-emphasize ($\gamma < 1$) the noise and signal statistics, respectively. The value of $\gamma$ must be chosen carefully for reliable deblurring. The choice of $\gamma$ is achieved through an iterative search (*8*). The uniqueness and convergence are uncertain and the restoration is sensitive to the initial image estimate. Combining an inverse filter with a weighting filter in a geometric mean filter (*10*) and the digital restoration in the wavelet domain approach (*11*) are also reported in the literature.

In this report, we design a practical deblurring filter that is less sensitive to the noise, while removing the blurring by a desired amount. We call it the P-deblurring filter because we utilize a special window, called a "power" window, to construct the deblurring filter. The deblurring process applies the P-deburring filter to the input image in the spatial frequency domain: the method does not require an iterative approach. Section 2 describes the structure of the P-deblurring filter. The design method, presented in section 3, utilizes the filter properties and estimates the energy of the signal and noise of the input image. The P-deblurring filter's performance is demonstrated by a human perception experiment which is described in section 4. The result analysis and conclusion are summarized in sections 5 and 6.

## 2. P-Deblurring Filter

The blurring function is usually a Gaussian-like function having a bell shape. The inverse function's magnitude increases at high frequencies where the noise can be magnified enormously. In order to suppress the noise effect, we apply a special window called a power window, to the inverse blurring function. The power window (*12*) is a Fourier-based smooth window that preserves most of the spatial frequency components in the passing band and attenuates quickly at the transition-band. The power window is differentiable at the transition point, which gives a desired smooth property and limits the ripple effect. A power window, and

a deblurring filter when applying the power window to a Gaussian blurring filter, are shown in figure 2. Our deblurring filter is called the P-deblurring filter because it was derived from utilizing the power window.

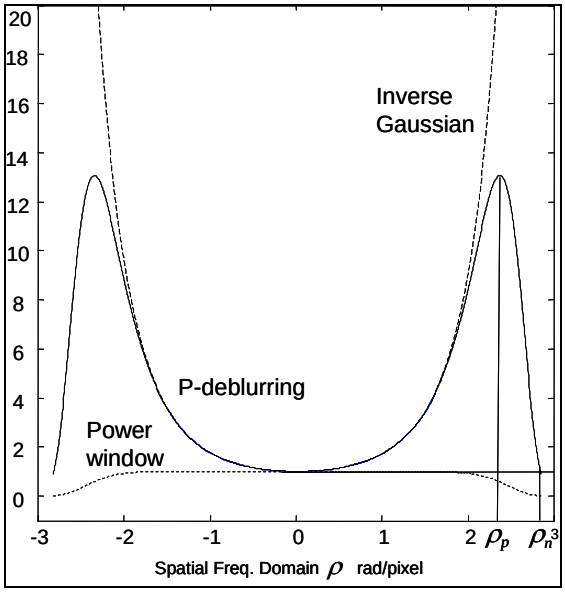


Figure 2. P-deblurring filter properties.

For a given blurring function $G(\rho)$, the P-deblurring filter $P(\rho)$ is written as:

$$P(\rho) = \frac{1}{G(\rho)} \cdot W(\rho) \tag{8}$$

where $W(\rho)$ is the power window. The power window is defined as follows:

$$W(\rho) = \exp(-\alpha\, \rho^n) \tag{9}$$

where the parameters ($\alpha$, $n$) are obtained based on certain specifications. Since the parameter $n$ is the power of the smooth window, this window is called power window. When we assume the Gaussian blurring function, the P-deblurring filter is defined as

$$P(\rho) = \frac{W(\rho)}{G(\rho)} = \exp(-\alpha\, \rho^n + \frac{\rho^2}{2\sigma^2}) \tag{10}$$

where $\sigma$ is the standard deviation of the Gaussian function.

## 3. P-Deblurring Filter Design

In this section, we describe the properties of the P-deblurring filter derived from the power window. Our design methods, of the P-deblurring filter based on these properties and user's specifications, are then proposed.

### 3.1 Properties of the P-Deblurring Filter

#### 3.1.1 The Peak Point

The P-deblurring filter has a maximum magnitude at peak point as shown in figure 2. This peak point is solved by setting the derivative of the P-deblurring filter zero. That is,

$$\frac{\partial P(\rho)}{\partial \rho}\Big|_{\rho_p} = 0 \quad \Rightarrow \quad \rho_p = (\alpha n \sigma^2)^{\frac{1}{2-n}}. \tag{11}$$

The maximum magnitude of the P-deblurring filter is an important parameter for the filter design. Here, the peak point $\rho_p$ is a function of three parameters ($\alpha$, $n$, $\sigma$). The filter design criteria are derived from specifying these parameters.

#### 3.1.2 The Noise Separation Frequency Point

Usually, the signal is stronger than noise in the low frequencies and weaker than noise in the higher frequencies. The noise is assumed to be a white process cross a wide range of the frequency. At one point, called the noise separation frequency point $\rho_n$, the signal and noise are equal as shown in figure 1b. The noise is stronger than the signal for frequencies greater than $\rho_n$.

One criteria of the filter design is to allow the magnitude of the P-deblurring filter to be 1 at the noise separation frequency point $\rho_n$ as shown in figure 2. In this way, the magnitude of the P-deblurring filter is less than 1 for frequencies greater than the noise separation frequency point $\rho_n$ where the noise is stronger than the signal. Meanwhile, the magnitude of the P-deblurring filter can be large below the noise separation frequency point $\rho_n$ where the signal is strong. This kind of deblurring filter provides the necessary deblurring. Therefore, the P-deblurring filter satisfies the following condition:

$$P(\rho) = \begin{cases} > 1, & if \ \rho < \rho_n; \\ = 1, & if \ \rho = \rho_n; \\ < 1, & if \ \rho > \rho_n. \end{cases} \tag{12}$$

If the SNR at the noise separation frequency point $\rho_n$ is estimated (see subsection 3.3), we can also solve three parameters ($\alpha$, $n$, $\sigma$) from (10) using $\rho_n$ and $P(\rho_n) = 1$.

### 3.1.3 The Cutoff Frequency Point

The cutoff frequency point of the power window, $\rho_0$, is where the magnitude of the power window attenuates significantly. This point has an important impact on the filter design since it controls when the inverse blurring function drops significantly. The cutoff frequency can also determine the shape of the power window by solving the two parameters ($\alpha$, $n$) (*12*).

## 3.2 Direct Design

In this section, we describe a direct design method of the deblurring filter which can benefit an imaging system that the sensor information and the noise characteristic are known. The direct design method is simple and easy to implement. The performance of this deblurring filter is predictable.

Assume the blurring function is a Gaussian function. We can specify the magnitude of the inverse Gaussian, *mg*, at one frequency point, $\rho_g$. This frequency point $\rho_g$ is calculated in the following:

$$\frac{1}{G(\rho_g)} = mg \qquad \Rightarrow \qquad \rho_g = \sigma\sqrt{2\ln(mg)} \tag{13}$$

where $\sigma$ is the standard deviation of the Gaussian function. The standard deviation of Gaussian $\sigma$ is either known or estimated by applying a curve fitting procedure to the ensemble magnitude spectrum (see subsection 3.3.1). If we choose the cutoff frequency point $\rho_0$ as $\rho_g$, the power window is constructed. The P-deblurring filter is finally determined from (9).

An example of applying the P-deblurring filter to one Forward-Looking Infrared (FLIR) tank image is shown in figure 3. Note the numbers of pixels in *x* and *y* domains are different. However, the spatial sampling spaces, $\Delta_x$ and $\Delta_y$, are the same. From the discrete Fourier transform (DFT) equation (*13*),

$$N_x \cdot \Delta_x \cdot \Delta_{k_x} = 2\pi \tag{14}$$

$$N_y \cdot \Delta_y \cdot \Delta_{k_y} = 2\pi \tag{15}$$

where $N_x$ and $N_y$ are the numbers of pixels in *x* and *y* domains, respectively; $\Delta_{k_x}$ and $\Delta_{k_y}$ are the sampling spaces in spatial frequency domains, respectively. Thus, $\Delta_{k_x}$ and $\Delta_{k_y}$ are not equal to each other. However, the support bands in the spatial frequency domains,

$$\pm K_{x0} = \pm \frac{\pi}{\Delta_x} \tag{16}$$

$$\pm K_{y0} = \pm \frac{\pi}{\Delta_y} \tag{17}$$

are equal to each other. For this reason, the spectral distributions shown in 3c and 3d are square shaped and not rectangular shaped as in the spatial domain image.

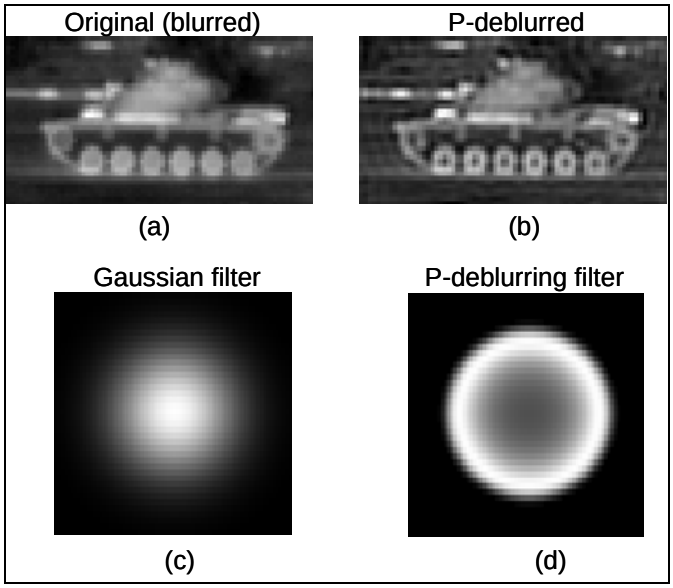


Figure 3. Example of the direct design for a FLIR tank image.

Note: (a) Original (blurred), and (b) P-deblurred images are illustrated in spatial domain. (c) Gaussian filter, and (d) P-deblurring filters are illustrated in spatial frequency domain.

We assume that this image is already blurred by a Gaussian function. By selecting

$$\sigma = 0.25 * \rho_{\max}, \qquad mg = 10 \tag{18}$$

where $\rho_{\max}$ is the maximum frequency of the Fourier transform of the input image. The original and P-deblurred tank images are shown figure 3a and 3b. The Gaussian blurring function and the resultant P-deblurring filter are shown in figure 3c and d. The deblurred tank clearly shows the deblurring improvement, especially around the tire area. Figure 4 shows the one-dimensional (1-D) cross section of each image in figure 3. The 1-D cross section of the tank image is a horizontal crossing line at the center of the tires. The deblurring effects show equally.

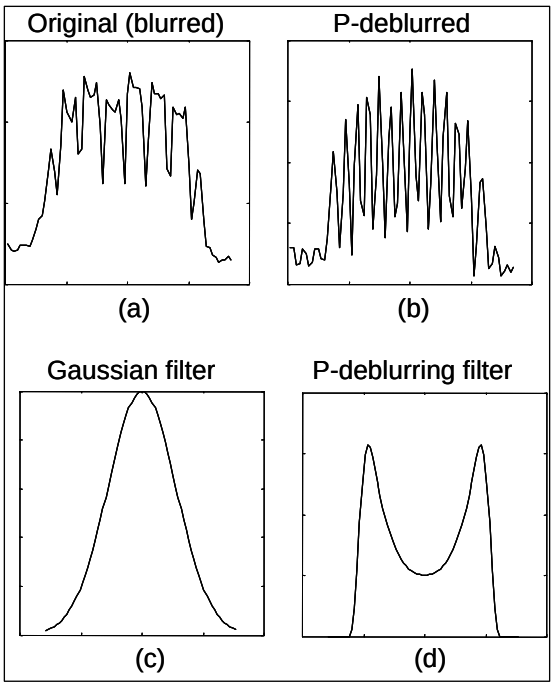


Figure 4. Cross sections of images in figure 3.

### 3.3 Adaptive Design

In this section, we describe a deblurring filter that is adaptively designed based on the estimated energy of the signal and noise of the image, which can benefit an imaging system with noise. The adaptive design estimates the noise energy and the noise separation frequency point where the energy of signal and noise are equal. The noise energy is stronger than the signal energy beyond that noise separation frequency point. The filter design criteria are defined to obtain a deblurring filter such that the filter magnitude is less than 1 at the frequencies above the noise separation frequency point; the filter magnitude is larger than 1 at the frequencies below the noise separation frequency point and the signal is strong as shown in (12). Therefore, the adaptively designed P-deblurring filter is able to deblur the image by a desired amount based on the known or estimated standard deviation of the Gaussian blurring while suppressing the noise in the output image.

#### 3.3.1 Estimating Noise Energy and Noise Separation Frequency Point

In this section, we outline a method to estimate the noise energy level in the spectral domain of the acquired image. Let $f(x, y)$ be the continuous input image. We define its 1-D marginal Fourier transform via

$$F_x(k_x, y) = \Im_{(x)}[f(x, y)]. \tag{19}$$

Now consider the image that is the discrete version of $f(x, y)$, that is, $f_{ij}, i = 1, \cdots, N, j = 1, \cdots, M$ . The 1-D DFT of this two-dimensional (2-D) array are discrete samples of $F_x(k_x, y)$ : $F_{ij}^{(i)}, i = 1, \cdots N, j = 1, \cdots M$. The ensemble magnitude spectrum, $S = [s_1, \cdots s_N]$, is computed via

$$s_i = \sqrt{\frac{1}{M}\sum_{j=1}^{M}\left|F_{ij}^{(i)}\right|^2}, \quad i = 1, \cdots N. \tag{20}$$

An example of the ensemble magnitude spectrum from one input FLIR image is shown in the upper left corner of figure 5a.

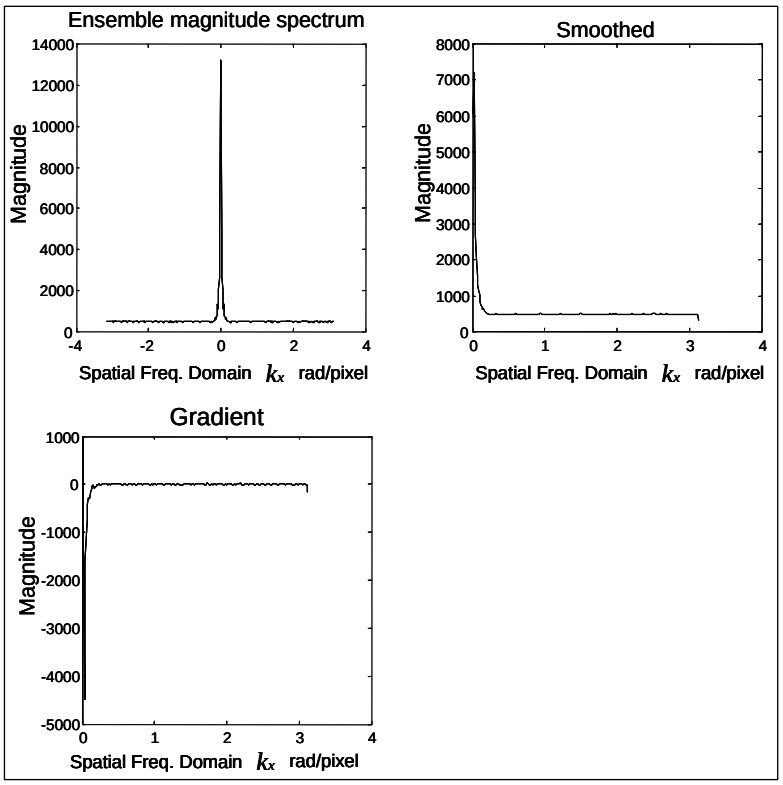


Figure 5. Ensemble magnitude spectrum of a FLIR image.

Usually, the signal is stronger than the noise at the low frequencies and weaker than the noise at the high frequencies. The same figure shows the ensemble magnitude spectrum remained unchanged after a high frequency point. The unchanged spectrum is mainly a noise spectrum since the noise dominates the signal at the very high frequencies. Furthermore, the noise is commonly a white process cross a wide range of frequencies. The noise separation frequency point is the frequency where the ensemble spectrum becomes unchanged (levels off).

In order to accurately estimate the noise separation frequency point, we first smooth the ensemble spectrum by convolving it with an averaging filter; denoted by *SM*:

$$SM = [sm_1, \cdots, sm_N]. \tag{21}$$

The averaging filter is chosen to be

$$[1 \quad 1 \quad 1]/3 \tag{22}$$

as an example. After this step, the gradient of the smoothed spectrum is computed as follows:

$$G_i = sm_{i+1} - sm_{i-1}. \tag{23}$$

Examples of the smoothed spectrum (5b) and its gradient curve for the positive frequencies (5c) are shown in figure 5. The gradient curve is searched from zero frequency to the positive frequencies. The search stops at a frequency point when the absolute value of the gradient is less than a threshold; we refer to this as the index frequency point. Note that the selection of this threshold is suggested to have the index frequency point to be at the beginning point when the ensemble spectrum levels off. The smooth filtering of the ensemble spectrum makes the threshold less sensitive to the noise.

The value of the ensemble magnitude spectrum at the index frequency point represents the noise energy; the value of the ensemble magnitude spectrum near the zero frequency point represents the signal energy. The SNR is computed as the ratio of the signal energy to the noise energy. Note the value of the ensemble magnitude spectrum at the zero frequency represents the direct current (DC) value of the image energy; therefore, the value is usually a very big number. The calculation of SNR should avoid using this value and instead use the value nearer the zero frequency point. Using the value of the ensemble magnitude spectrum, that is 1–2 pixels from zero frequency, is a good practice.

The spectrum of an ideal (point) target is flat; however, the acquired spectrum of a target is decayed due to the blurring function. At the index frequency point, the acquired signal value is $1/SNR$ if the ideal signal is 1. The noise separation frequency point $\rho_n$ is calculated as follows:

$$\rho_n = \sigma\sqrt{2\ln(SNR)}, \tag{24}$$

where $\sigma$ is the standard deviation of the Gaussian function.

### 3.3.2 Filter Design

The overall goal of the deblurring filter is to provide the satisfied output image, i.e., the proper deblurring and the proper noise control. This goal can be achieved by adaptively determining the proper parameters of the deblurring filter based on estimated noise energy of the input image.

As earlier stated, to construct the P-deblurring filter we need to determine three parameters ($\alpha$, $n$, $\sigma$). From the discussion above, the standard deviation of Gaussian $\sigma$ is either known or estimated by applying a curve fitting procedure to the ensemble magnitude spectrum. By specifying two distinct values of $P(\rho)$ as shown in (9), we can solve for the other two parameters ($\alpha$, $n$). For example, one can select:

$$\begin{aligned} P\ |_{\rho_1 = \rho_n} &= 1, \\ P\ |_{\rho_2 = 0.8\rho_n} &= W_2. \end{aligned} \tag{25}$$

This means that the magnitude of the P-deblurring filter is set to 1 at the noise separation frequency point, and the magnitude is set to $W_2$ ($W_2 > 1$) at 80% of the noise separation frequency point.

However, the selection of $W_2$ is not completely arbitrary. Because the power window is less than 1, the magnitude of the P-deblurring filter is less than the inverse Gaussian function, that is,

$$W_2 < \exp(\frac{\rho_2^2}{2\sigma^2}). \tag{26}$$

Therefore, $W_2$ is chosen according to this condition. There are other procedures to determine the other two parameters ($\alpha$, $n$). Caution must be used when determining these parameters, since the conditions of P-deblurring filter need to be met. An example of applying the adaptive design P-deblurring filter to a FLIR image is shown in section 4.

---

## 4. Perception Experiment

---

In order to assess the performance of our proposed adaptive deblurring filter method, a perception experiment was conducted to demonstrate the P-deblurring filter effect on the target identification task of humans. The image set consisted of 12 standard targets taken from a field test by Night Vision and Electronic Sensors Directorate (NVESD) using a longwave infrared sensor. The targets in the set are well-characterized in terms of predicting range performance based upon sensor characteristics. The side views of these 12 targets (at the aspect angle $90^\circ$ or $270^\circ$) are depicted in figure 6. Each target, posing at 12 aspect angles, makes the total image set contain 144 images of 12 different targets.

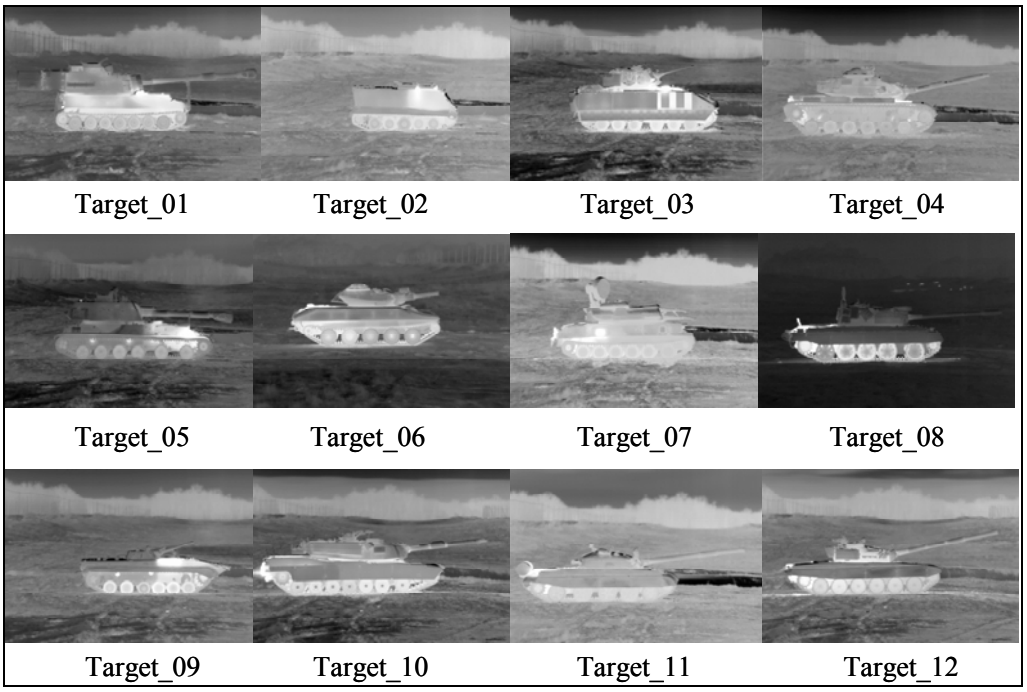


Figure 6. Thermal image examples for 12-target sets.

Experimental cell organization was based on three factors. First, images were subjected to six levels of blur to simulate range effects on identification task difficulty. Second, images were subjected to three different noise treatments in order to test the effectiveness of the deblurring algorithm on noisy images. Third, each of the cells was processed using the deblurring algorithm to quantify differences between blurred and deblurred image cases as a function of blur. An illustration of the experimental matrix layout and naming convention is shown in table 1.

Table 1. Experiment matrix layout and naming convention.

| | **Blur 1** | **Blur 2** | **Blur 3** | **Blur 4** | **Blur5** | **Blur 6** |
|---|---|---|---|---|---|---|
| **Noise0 Blur** | AA | AB | AC | AD | AE | AF |
| **Noise0 Deblur** | BA | BB | BC | BD | BE | BF |
| **Noise1 Blur** | CA | CB | CC | CD | CE | CF |
| **Noise1 Deblur** | DA | DB | DC | DD | DE | DF |
| **Noise2 Blur** | EA | EB | EC | ED | EE | EF |
| **Noise2 Deblur** | FA | FB | FC | FD | FE | FF |

The total 144 images in the first row are arranged into six blur cells in the following manner. The aspect angles were rotated through the blur cells so that each cell had the same number of images at a particular aspect angle. Within each blur cell, there are 24 target images that have various aspect angles of 12 different targets. It should be noted that the target images within a particular blur in the first row are the same target images for that particular blur in the noise adding and deblurring cells in the same column.

Figure 7 shows Gaussian filters with six values of standard deviations that were applied to imagery to generate blurred images. These six standard deviations of Gaussian filters were chosen to vary the observer performance, from a very high probability of a correct answer to a very low probability of a correct answer, with equally decreasing increment.

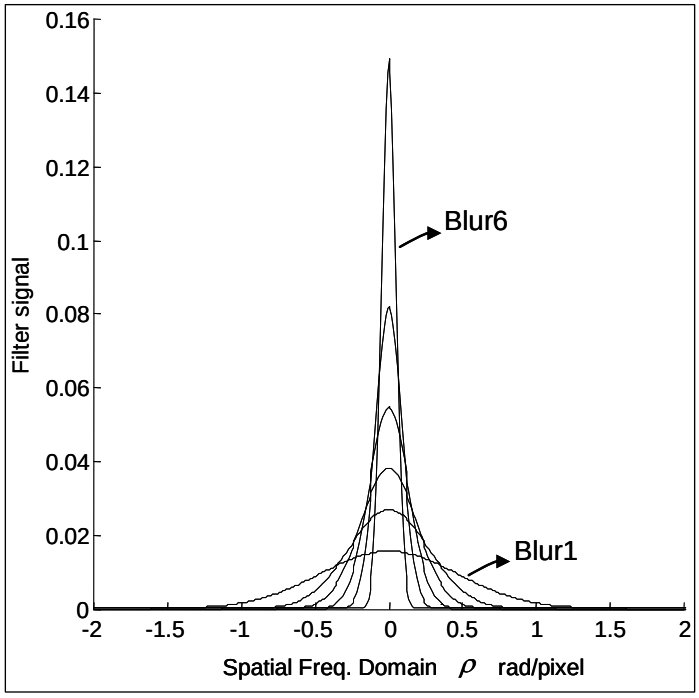


Figure 7. Gaussian function in frequency domain.

Three noise treatments followed. First, there was no additional noise added to the blurred images. This case is considered a low noise situation, and noted as Noise0. For the other two noise treatments, two levels of white noise were added to the blurred images. A white noise with a standard deviation of 100 millikelvin (mK) is added to a typical infrared image, which has the signal to noise ratio of 20 K and considered to be the upper bound of noise. Based on this, the second noise case, noted as Noise1, is chosen to be a white noise with a standard deviation of 50 mK, which is a typical noise situation. The third noise case, noted as Noise2, is the white noise with a standard deviation of 100 mK, which is an upper bound noise situation. An image that was blurred with blur level 6 and the blurred image with added noise are shown in the first row of figure 8. The P-deblurred resultant images are shown in the second row of figure 8. The P-deblurred images demonstrate deblurring improvement from their blurred input images,

especially, when the noise added in the blurred image is suppressed in the deblurred output image, which benefits from the adaptive design method.

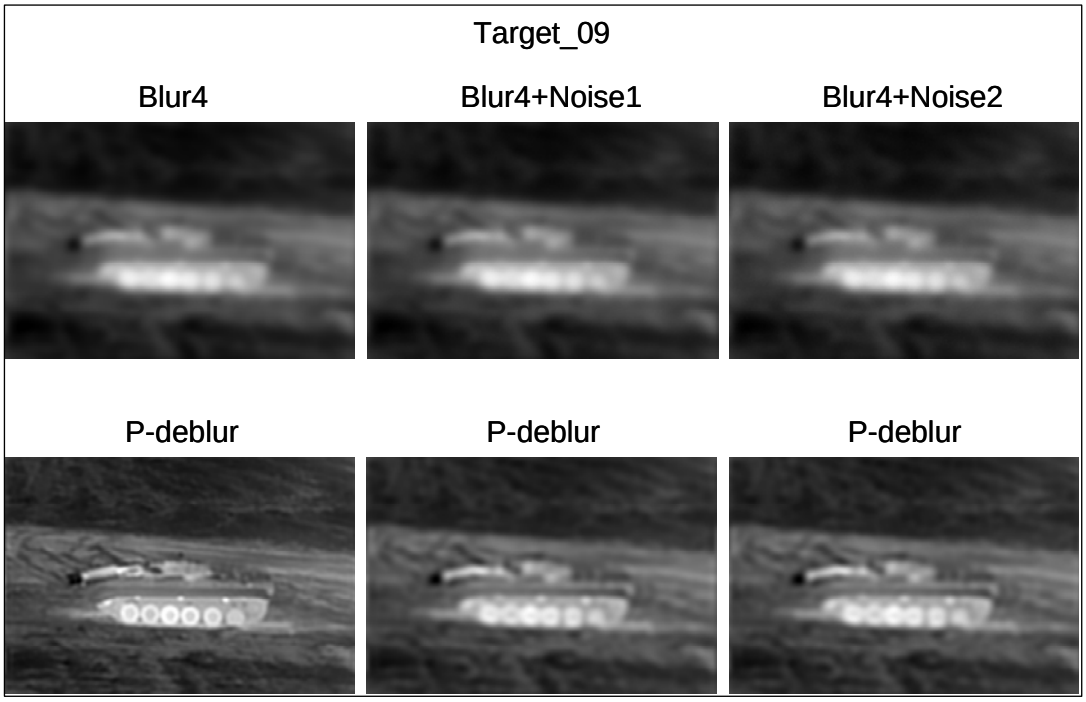


Figure 8. Sample examples of blurred, blurred with noise, and P-deblurred images.

Ten observers were trained using the ROC-V Thermal Recognition software to identify the 12 target set as presented in the experiment. Each observer was trained to a 96% proficiency in identification of pristine images at various ranges. This proficiency requirement prevents potentially biased results stemming from subjects learning target specific characteristics during the testing process.

Experimental trials were conducted using a high resolution, medical grade display in order to allow for accurate representation of image characteristics. For consistency, the displays were all calibrated between experimental setups using a Prichard model 1980 spot photometer to ensure (realistically) identical minimum, mean, and peak luminance. Each display was calibrated to a mean level of 5.81 foot-Lamberts. Experimental trials were conducted in a darkened environment and observers were given ample time to adapt to ambient lighting conditions.

## 5. Result Analysis

The average probabilities of identification from the experiment, *P*, were adjusted using the following equation

$$P_{id} = \frac{P - P_g}{P_s - P_g}, \quad P_g = \frac{1}{12}, \quad P_s = \frac{9}{10} \tag{27}$$

to remove the probability that an observer could select the proper response simply through guessing 1 out 12 targets. Previous experimental analysis indicates that the inclusion of a "sweat factor"normalizes probabilities to 90% for inclusion of a 10% mistake rate. For the typical observer this normalization provides a more accurate reflection of observer performance by accounting for mistakes and unfamiliarity with the testing environment.

The adjusted probability of identification $P_{id}$ as a function of blur (range) for the different cases is shown in figure 9. There was a significant improvement in human performance, as a function of range, when the blurred imagery was processed using the P-deblurring filter. Noise0 Blur images are considered as the "baseline" images. For the blur level 1–3 (near range), the $P_{id}$ of the baseline images is high (60% to 90%). However, for the blur level 4–6 (long range), the $P_{id}$ of the baseline images is very low (10% to 30%); that is where the P-deblurring filter's improvement takes place (38% to 65%). For the blur level 4–6, the average increase of $P_{id}$ is 33% by using deblurred images vs. blurring images in the Noise0 case (figure 9a); the average increase of $P_{id}$ is 15% in the Noise1 case (figure 9b). In the Noise2 case, the improvement of $P_{id}$ is negligible using the deblurred images (figure 9c). In summary, the $P_{id}$ is increased 15% to 33% for the case of typical noise to low noise in the long range using the P-deblurring filter method.

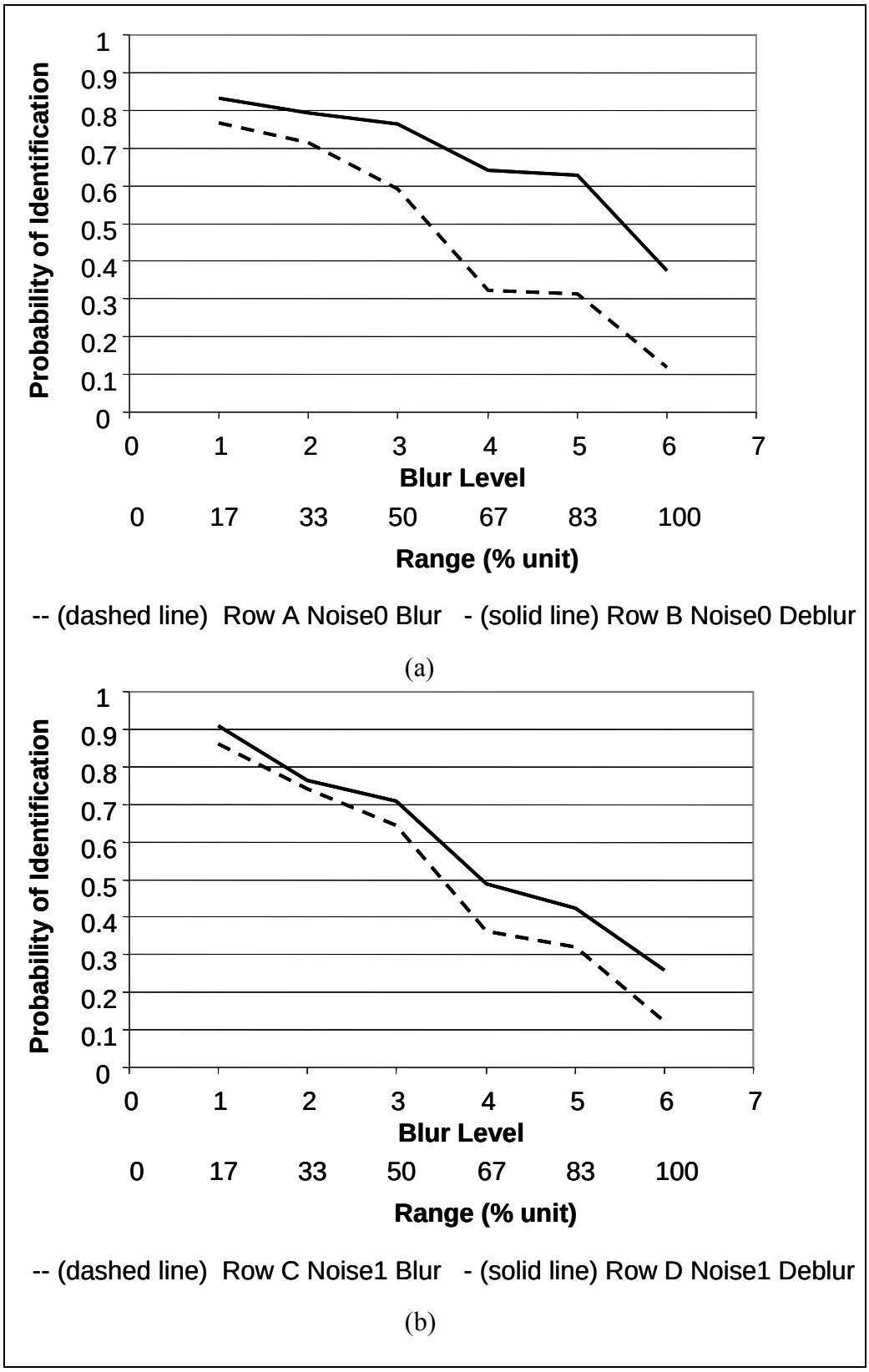


Figure 9. (a) Perception results of Noice0 blur vs. Noise0 deblur, and (b) perception results of Noise1 blur vs. Noise1 deblur.

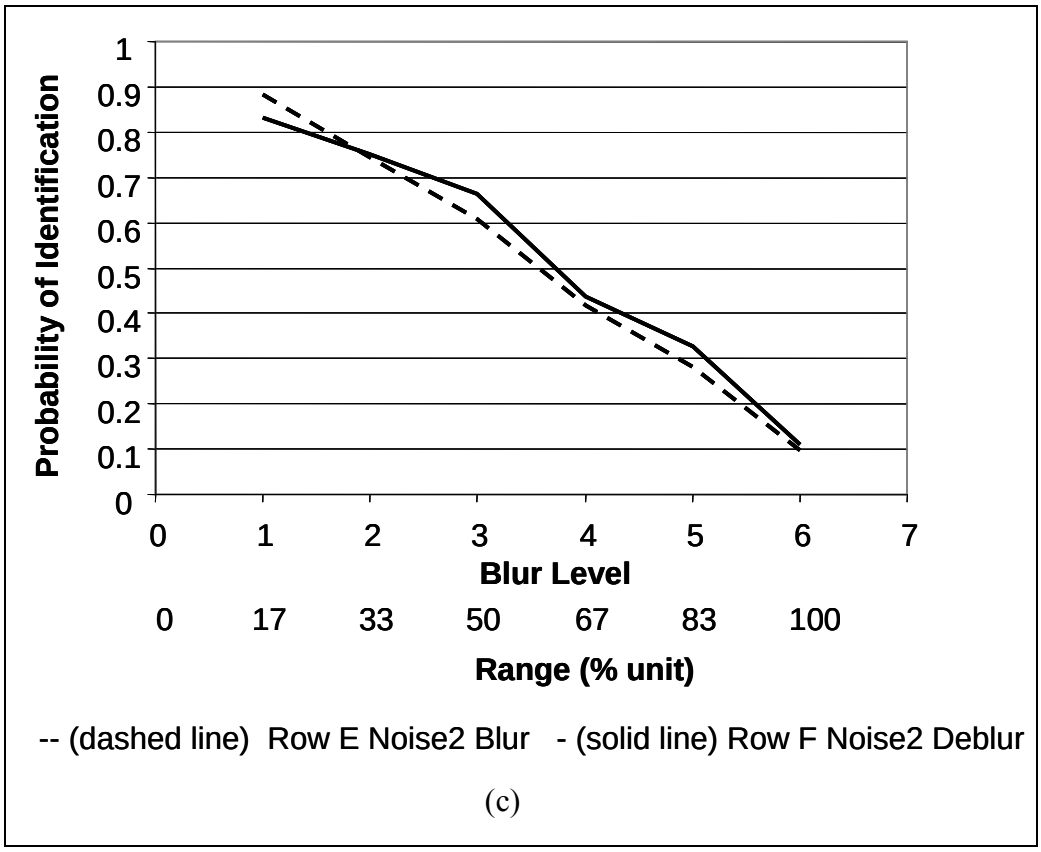


Figure 9. (c) Perception results of Noise2 blur vs. Noise2 deblur.

In order to estimate the range performance, we assume the range is linearly increased with the increasing blur level since the chosen blurs generate equal increment blur effect on the images. In figure 9a, the Noise0 case, blurring imagery had a 50% $P_{id}$ at the range 55% unit (blur level 3.3), while the P-deblurred imagery reached the range 92% unit (blur level 5.5) for the 50% $P_{id}$. That is equivalent to 67% increase in range performance. Similarly, in the Noise1 case shown in figure 9b, P-deblurred imagery yielded the range 67% unit (blur level 4) comparing with the range 58% unit (blur level 3.5) from the blurring imagery at 50% $P_{id}$. That is about 16% increase in range performance. In the Noise2 case, at 50% $P_{id,}$ the range is at 63% unit (blur level 3.8) for P-deblurring imagery comparing with 58% unit (blur level 3.5) from blurring imagery, which is a 9% increase in range performance. In summary, the range performance is increased 9%, 16%, and 57% for the case of upper bound noise, typical noise, and low noise in the input images, respectively, using the P-deblurring filter method. This quantitative analysis of the range performance is estimated approximately. The accurate analysis will be based on accurate range calculation. The ideal case would acquire the imagery using real range images, which is our plan for future research.

## 6. Conclusions

This report proposes an adaptive deblurring filtering algorithm for noisy images. The algorithm is practical, Fourier-based, and can be implemented in real-time. The improvement using this algorithm for noisy blurring images is demonstrated in a human perception experiment of the target identification task. The potential benefit of this practical deblurring algorithm is that it can be implemented into a real imaging system to compensate the sensor blurring and noise effect on its output images. Another potential benefit is that if other blur sources such as motion, vibrations, or atmosphere can be modeled as a Modulation Transfer Function (MTF), the proposed adaptive deblurring filtering algorithm can still be applied. Since the power window can be applied to a known inversed MTF, with respect to the estimated blur and noise, the noise can be suppressed in the deblurring process while the deblurring can be performed effectively. The proposed adaptive deblurring filtering method will work well in the cases, even when MTF is not monotonically decreasing, as long as the inverse of MTF is valid.

## References


1. Andrews, H.C.; Hunt, B.R. *Digital Image Restoration*; Englewood Cliffs, NJ: Prentice-Hall, 1977.
2. Frieden, B.R. Image enhancement and restoration*, In Picture Processing and Digital Processing,* T.S. Huang, Ed., pp 177–248, Berlin: Spring-Verlag, 1975.
3. Blass, W.E.; Halsey, G.W. *Deconvolution of Absorption Spectra*; New York, NY: Academic Press, 1981.
4. Demoment, G. Image reconstruction and restoration: overview of common estimation structures and problems. *IEEE Trans. on Acoustics, Speech, and Signal Processing*. **1989**, *37*, 2024–2036.
5. Kundur, D.; Hatzinakos, D. Blind Image Deconcolution. *IEEE Signal Processing Magazine.* **1996**, 43–64.
6. Lagendijk, R.L.; Tekal, A.; Biemond, J. Maximum likelihood image and blur identification: a unifying approach. *Optical Engineerin.* **1990**, *29*, 422–435.
7. Sezan, M.I.; Tekalp, A.M. Tutorial review of recent developments in digital image restoration. *In Visual Communications and Image Processing 1990*, M. Kunt, Ed., Proc. SPIE 1360, 1346–1359, 1990.
8. Gerwe, D.R.; Jain, M.; Calef, B.; Luna, C. Regularization for non-linear image restoration using a prior on the object power spectrum. *Proceedings of SPIE Vol. 5896, Unconventional Imaging,* pp 1–15, 2005.
9. Mateos, J.; Molina, R.; Katsaggelos, A.K. Approximation of posterior distributions in blind deconvolution using variational methods. *Proceedings of IEEE ICIP*, pp II-770:II-773, 2005.
10. Stern, A.; Kopeika, N.S. General restoration filter for vibrated-image restoration. *Applied Optics.* **1998**, *37*, 7596–7603.
11. Lam, E. Digital restoration of defocused images in the wavelet domain. *Applied Optics.* **2002**, *41*, 4806–4811.
12. Young, S.S. Alias-free image subsampling using Fourier-based windowing methods. *Optical Engineering.* **2004**, *43*, 843–855.
13. Soumekh, M. *Fourier Array Imaging*; Englewood Cliffs, NJ: Prentice-Hall, 1994.

## Acronyms and Abbreviations

| | |
|---|---|
| DC | direct current |
| DFT | discrete Fourier transform |
| EM | expectation-maximization |
| FLIR | Forward-Looking Infrared |
| K | kelvin |
| LSI | Linear Shift Invariant |
| MAP | maximum a posterior |
| mK | millikelvin |
| MTF | Modulation Transfer Function |
| NVESD | Night Vision and Electronic Sensors Directorate |
| PSF | point spread function |
| RMSE | root mean square error |
| SNR | signal to noise ratio |
| 1-D | one-dimensional |
| 2-D | two-dimensional |

## Distribution List

| No. Copies | Organization |
|---|---|
| 1 (PDF COPY) | ADMNSTR<br>DEFNS TECHL INFO CTR<br>ATTN DTIC OCP<br>8725 JOHN J KINGMAN RD STE 0944<br>FT BELVOIR VA 22060-6218 |
| 2 | DARPA<br>ATTN IXO S WELBY<br>ATTN J RICKLIN<br>3701 N FAIRFAX DR<br>ARLINGTON VA 22203-1714 |
| 1 | NGA<br>ATTN R S RAND<br>12310 SURSISE VALLEY DR<br>MAIL STOP DN 11<br>RESTON VA 20191-3449 |
| 1 | OFC OF THE SECY OF DEFNS<br>ATTN ODDRE (R&AT)<br>THE PENTAGON<br>WASHINGTON DC 20301-3080 |
| 1 | US ARMY RSRCH DEV AND ENGRG CMND<br>ARMAMENT RSRCH DEV AND ENGRG CTR<br>ARMAMENT ENGRG AND TECHNLGY CTR<br>ATTN AMSRD AAR AEF T J MATTS<br>BLDG 305<br>APG MD 21005-5001 |
| 2 | US ARMY TRADOC<br>BATTLE LAB INTEGRATION & TECHL DIRCTRT<br>ATTN ATCD B<br>ATTN ATCH B<br>10 WHISTLER LANE<br>FT MONROE VA 23651-5850 |
| 1 | US MILITARY ACDMY<br>MATHEMATICAL SCI CTR OF EXCELLENCE<br>ATTN MAJ J HARTKE<br>PHOTONICS CENTER<br>WEST POINT NY 10996-1786 |
| 1 | PRODUCT MANAGER TIMS<br>ATTN SFAE IEWS NS TIMS<br>B GRIFFIES<br>BLDG 563<br>FT MONMOUTH NJ 07703 |
| 1 | SMC/GPA<br>2420 VELA WAY STE 1866<br>EL SEGUNDO CA 90245-4659 |
| 1 | US ARMY ABERDEEN TEST CENTER<br>ATTN CSTE DT AT WC A F CARLEN<br>400 COLLERAN ROAD<br>APG MD 21005-5009 |
| 1 | US ARMY ABERDEEN TEST CENTER<br>ATTN CSTE DTC AT TC N<br>D L JENNINGS<br>400 COLLERAN ROAD<br>APG MD 21005-5059 |
| 1 | US ARMY ERDC<br>ATTN CEERD TR S<br>7701 TELEGRAPH RD BLDG 2592<br>ALEXANDRIA VA 22315 |
| 1 | US ARMY INFO SYS ENGRG CMND<br>ATTN AMSEL IE TD F JENIA<br>FT HUACHUCA AZ 85613-5300 |
| 3 | US ARMY MATERIEL SYS ANAL ACTVTY<br>ATTN AMSRD AMS SC G KISTNER<br>ATTN AMSRD AMS SC J MAZZ<br>ATTN AMSRD AMS SC R WHEELER<br>392 HOPKINS RD<br>APG MD 21005-5071 |
| 1 | US ARMY NATICK RDEC<br>ACTING TECHL DIR<br>ATTN SBCN TP P BRANDLER<br>KANSAS STREET BLDG 78<br>NATICK MA 01760-5056 |

| No. Copies | Organization |
|---|---|
| 1 | US ARMY PM NV/RSTA<br>ATTN SFAE IEW&S NV<br>10221 BURBECK RD<br>FT BELVOIR VA 22060-5806 |
| 1 | COMMANDER<br>US ARMY RDECOM<br>ATTN AMSRD AMR W C MCCORKLE<br>5400 FOWLER RD<br>REDSTONE ARSENAL AL 35898-5000 |
| 1 | US ARMY RDECOM AMRDEC<br>ATTN ATCD B<br>FT MONROE VA 23651-5850 |
| 2 | US ARMY RDECOM AMRDEC<br>ATTN AMSRD AMR SG W PITTMAN<br>ATTN AMSRD AMR SG IP<br>H F ANDERSON<br>BLDG 5400<br>REDSTONE ARSENAL AL 35809 |
| 1 | US ARMY RDECOM AMRDEC<br>ATTN AMSRD AMR SG IR R SIMS<br>BLDG 5400<br>REDSTONE ARSENAL AL 35898 |
| 1 | US ARMY RDECOM AMRDEC<br>ATTN AMSRD AMR WS PL<br>W DAVENPORT<br>BLDG 7804<br>REDSTONE ARSENAL AL 35898 |
| 2 | US ARMY RDECOM ARDEC<br>ATTN AMSRD AAR AEP S<br>P WILLSON<br>ATTN AMSRD AAR AER S<br>J ROMANO<br>RADIOGRAPHIC LABORATORY B 908<br>PICATINNEY ARSENAL NJ 07806-5000 |
| 4 | US ARMY RDECOM CERDEC NVESD<br>ATTN AMSRD CER NV MS<br>R DRIGGERS<br>ATTN AMSRD CER NV OD<br>J RATCHES<br>ATTN AMSRD CER NV ST J HILGER<br>ATTN AMSRD CER NV ST<br>P PERCONTI<br>10221 BURBECK RD STE 430<br>FT BELVOIR VA 22060-5806 |

| No. Copies | Organization |
|---|---|
| 1 | US ARMY RDECOM TARDEC<br>ATTN AMSRD TAR R G R GERHART<br>6501 E ELEVEN RD MS 263<br>WARREN MI 48397-5000 |
| 1 | US ARMY RSRCH LAB<br>ATTN AMSRD ARL CI OK TP<br>TECHL LIB T LANDFRIED<br>BLDG 4600<br>APG MD 21005-5066 |
| 4 | DIRECTOR<br>US ARMY RSRCH LAB<br>ATTN AMSRD ARL RO EL L DAI<br>ATTN AMSRD ARL RO M D ARNEY<br>ATTN AMSRD ARL RO MI<br>R ZACHERY<br>ATTN AMSRD ARL RO MM<br>M-H CHANG<br>PO BOX 12211<br>RESEARCH TRIANGLE PARK NC<br>27709-2211 |
| 1 | US ARMY SOLDIER & BIO CHEM CTR<br>ATTN AMSSB RT P W LOEROP<br>EDGEWOOD CHEM & BIO CTR<br>BLDG E 5554<br>APG MD 21010-5424 |
| 1 | COMMANDER<br>USAISEC<br>ATTN AMSEL TD BLAU<br>BUILDING 61801<br>FT HUACHUCA AZ 85613-5300 |
| 1 | AFRL/SNAA<br>ATTN M JARRATT<br>2241 AVIONICS CIRCLE AREA B<br>BLDG 620<br>WRIGHT PATTERSON AFB OH<br>45433-7321 |
| 1 | CMTCO<br>ATTN MAJ A SUZUKI<br>1030 S HIGHWAY A1A<br>PATRICK AFB FL 23925-3002 |

No. Copies | Organization

1 US GOVERNMENT PRINT OFF
DEPOSITORY RECEIVING SECTION
ATTN MAIL STOP IDAD J TATE
732 NORTH CAPITOL ST NW
WASHINGTON DC 20402

3 SITAC
ATTN H STILES
ATTN K WHITE
ATTN R DOWNIE
11981 LEE JACKSON MEMORIAL HWY
SUITE 500
FAIRFAX VA 22033-3309

1 US ARMY RSRCH LAB
ATTN AMSRD ARL WM BF G HAAS
APG MD 21005-5067

1 US ARMY RSRCH LAB
ATTN AMSRD ARL WM BF
W OBERLE
BLDG 390
APG MD 21005-5067

1 DIRECTOR
US ARMY RSRCH LAB
ATTN AMSRD ARL RO EV
W D BACH
PO BOX 12211
RESEARCH TRIANGLE PARK NC 27709

11 US ARMY RSRCH LAB
ATTN AMSRD ARL CI OK T
TECHL PUB (2 COPIES)
ATTN AMSRD ARL CI OK TL
TECHL LIB (2 COPIES)
ATTN AMSRD ARL D J M MILLER
ATTN AMSRD ARL SE
J PELLEGRINO
ATTN AMSRD ARL SE S J EICKE
ATTN AMSRD ARL SE SE
N NASRABADI
ATTN AMSRD ARL SE SE
P GILLESPIE
ATTN AMSRD ARL SE SE
S S YOUNG
ATTN IMNE ALC IMS
MAIL & RECORDS MGMT
ADELPHI MD 20783-1197

TOTAL: 60 (59 HCs and 1 Electronic)

INTENTIONALLY LEFT BLANK.